Peptide Folding, Metal-Binding Mechanisms, and Binding Site Structures in Metallothioneins

KELLY E. RIGBY DUNCAN, THANH T. NGU, JAYNA CHAN, MARIA T. SALGADO, MAUREEN E. MERRIFIELD, AND MARTIN J. STILLMAN[1]

Department of Chemistry, The University of Western Ontario, London, Ontario, Canada N6A 5B7

This minireview specifically focuses on recent studies carried out on structural aspects of metal-free metallothionein (MT), the mechanism of metal binding for copper and arsenic, structural studies using x-ray absorption spectroscopy and molecular mechanics modeling, and speciation studies of a novel cadmium and arsenic binding algal MT. Molecular mechanics–molecular dynamics calculations of apo-MT show that significant secondary structural features are retained by the polypeptide backbone upon sequential removal of the metal ions, which is stabilized by a possible H-bonding network. In addition, the cysteinyl sulfurs were shown to rotate from within the domain core, where they are found in the metallated state, to the exterior surface of the domain, suggesting an explanation for the rapid metallation reactions that were measured. Mixing $Cu_6\beta$-MT with $Cd_4\alpha$-MT and $Cu_6\alpha$-MT with $Cd_3\beta$-MT resulted in redistribution of the metal ions to mixed metal species in each domain; however, the Cu^+ ions preferentially coordinated to the β domain in each case. Reaction of As^{3+} with the individual metal-free β and α domains of MT resulted in three As^{3+} ions coordinating to each of the domains, respectively, in a proposed distorted trigonal pyramid structure. Kinetic analysis provides parameters that allow simulation of the binding of each of the As^{3+} ions. X-ray absorption spectroscopy provides detailed information about the coordination environment of the absorbing element. We have combined measurement of x-ray absorption near edge structure (XANES) and extended x-ray absorption fine structure (EXAFS) data with extensive molecular dynamics calculations to determine accurate metal-thiolate structures. Simulation of the XANES data provides a powerful technique for probing the coordination structures of metals in metalloproteins. The metal binding properties of an algal MT, *Fucus vesiculosus*, has been investigated by UV absorption and circular dichroism spectroscopy and electrospray ionization–mass spectrometry. The 16 cysteine residues of this algal MT were found to coordinate six Cd^{2+} ions in two domains with stoichiometries of a novel Cd_3S_7 cluster and a β-like Cd_3S_9 cluster. Exp Biol Med 231:1488–1499, 2006

Key words: protein folding; MM/MD; Cd(II), Zn(II), Cu(I), As(III); emission spectroscopy; metal domain; *Fucus vesiculosus*; kinetic analysis; EXAFS; XANES

Introduction

The first decades following the initial discovery of metallothionein (MT) focused largely on the properties of the metallated protein, as this was believed to be the only functionally relevant form. Several books and reviews were published in this period that described the results of a wide range of experiments; these included four conference reports (1–4), a specific volume of the *Methods in Enzymology* (5), a report from a specialist Pacifichem meeting in 1989 (6), and a wide-ranging review of spectroscopic properties (7). Studies in our laboratory have focused on characterizing the structural and electronic properties of the protein through both steady-state and kinetic analyses.

Despite the wide attention to MTs from many sources, the metal-free apo-MT has received the least study up until about 5 years ago. Circular dichroism (CD) spectra of the metal-free protein were interpreted as showing it to be a random coil with no secondary structural features. Indeed, because of the lack of absorption bands in the 230- to 300-nm range from aromatic residues, the CD spectrum was essentially flat above 220 nm in the absence of metals (6). Even below 200 nm, CD was found to be weak and relatively featureless. This apparent lack of structure in addition to a short lifetime in the cell resulted in very little interest in the metal-free state of the protein (8). A recent report, however, has provided evidence for the existence of a stable apo-MT species in quantities equaling that of the metallated protein in the liver, brain, and kidneys of rats (9). In light of this recent evidence, the current view has begun to shift to accept the possibility of apo-MT having a functional role *in vivo* and, therefore, the apo form may indeed possess structural features not previously recognized. We describe below our

This work was funded by the Natural Sciences and Engineering Research Council (NSERC) of Canada to M.J.S., and by graduate research scholarships to K.E.R.D. (NSERC), M.T.S. (Ontario Graduate Scholarship in Science and Technology [OGSST]), T.T.N. (Ontario Graduate Scholarship Program [OGS]), M.E.M. (OGS/OGSST), and J.C. (OGSST). This paper describes in part collaborative research with Prof. P. Norton at the University of Western Ontario and Prof. A. Soldatov at the University of Rostov.

[1] To whom correspondence should be addressed at Department of Chemistry, The University of Western Ontario, London, ON, Canada, N6A 5B7. E-mail: martin.stillman@uwo.ca

1535-3702/06/2319-1488$15.00

studies on the role of apo-MT in the metabolism of metals; that is, in the chaperone role that MT may well play in cells.

A second area of active research into the metal binding properties of MTs concerns the mechanism and structural aspects of metal binding to MTs. Included in these studies is the mechanism of the actual formation of metal-cys(-thiolate) clusters using the specific spectroscopic signatures of (i) cadmium (Cd), (ii) copper (Cu), (iii) silver (Ag), (iv) mercury (Hg), and recently (v) arsenic (As) structural probes. For example, we have approached the mechanistic studies by exploiting the specific emission of Ag(I) and Cu(I) bound to the cysteinyl sulfurs. Under these conditions both the emission intensity and the band maximum wavelength (λ_{max}) change as a function of the coordination environment. For Cu(I) binding we can relate the number and type of coordinating ligands, together with the extent of solvent access to the static and dynamic spectroscopic properties. Therefore, we have taken advantage of these specific Cu-thiolate optical emission properties of Cu-substituted α and β domains of MT to detect the preferential binding of Cu^+ to the β domain of MT as a function of time, and we use emission properties of Cu-MT (intensity and band maxima, λ_{max}) to determine the stoichiometric distribution of Cu^+ ions between the α and β domains of MT as a function of time. The binding properties of each isolated domain are correlated to the behavior of the two-domain protein, leading to a proposal of a unique pathway for the formation of the Cu_6S_9-β and Cu_6S_{11}-α clusters in MT.

Arsenic contamination is becoming a growing concern in many nations around the world. In India and Bangladesh, arsenic contamination of drinking water has reached a point of crisis (10, 11).

As^{3+} binds nonspecifically to sulfhydryl groups in proteins and enzymes, which is believed to deplete glutathione in the cell, leading in part to As toxicity (12). MT, consisting of 20 cysteine residues, would be an attractive target for As^{3+} binding.

Directly connected with the mechanism is the structure of the metal-thiolate clusters that form and influence of the peptide chain that surrounds the binding site on the stability of the metal clusters. Molecular modeling has proven to be a very effective and successful tool for predicting protein structure, either in conjunction with experimental data from common structural probes, or as a theoretical method. As computers become increasingly more powerful, molecular modeling calculations can be applied to larger and larger protein systems. This technique utilizes the information determined from experimental data to calculate molecular representations of the structure with a specific coordination environment (ligand type or types, and geometry adopted). From these structures it is then possible in some cases to further calculate and predict the spectroscopy, reactivity, transition states, and intermolecular interactions of these molecules (13, 14). X-ray absorption spectroscopy (XAS) is a very sensitive probe of metal coordination geometry. X-ray absorption fine structure (XAFS) spectra are extremely specific to the nature of the metal coordination site, yet the complexities of the scattering are not always easy to interpret. The periodicity of each spectrum provides information about the distance between the scattering atom and its neighbors, and the edge profiles of each spectrum can be used to determine coordination numbers.

Finally, MTs have been discovered in a wide range of organisms. The native metallation status provides information that connects structure with function in these organisms. We have studied the metal-binding properties of an algal MT from the brown seaweed *Fucus vesiculosus* (15), which grows in waters with high concentrations of Group 11 and 12 metals.

Therefore, this review comprises four sections: studies of metal-free MT, the mechanism of metal binding for copper and arsenic, structural studies, and studies of an algal MT.

Studies of Metal-Free MTs

The x-ray crystal structure of the metallated rat MT (16), as well as ^{111,113}Cd-nuclear magnetic resonance (NMR) structures of the metallated rabbit MT (17, 18), have demonstrated for the mammalian proteins a well-conserved metal-thiolate core within each of the α and β domains. The folding of each independent domain is induced by metal coordination to the cysteinyl sulfurs as either bridging or terminal ligands so that, unusually, the metallated protein has a secondary structure dominated by the metal binding. The intrinsic cross-linking of the metal centers to the cysteine residues requires complete synthesis of the protein backbone prior to folding. This implies that metallation and folding are post-translational events following *de novo* synthesis in the cell and, therefore, the apo-protein must initially exist *in vivo* (19).

Detecting possible structural conformations that may lead to specific secondary structure of the apo-MT *in vivo* or *in vitro* is extremely difficult due to the lack of the primary spectroscopic probe induced by the metal-thiolate bond. Molecular modeling is a practical alternative for the exploration of stable conformations of the metal-free protein. Classical molecular modeling, based on Newtonian physics, is one of the computational methods commonly used to calculate large molecular systems such as proteins, because this method is far less computationally expensive compared with quantum mechanical *ab initio* and semiempirical methods. However, the classical method will only provide reliable results if the force field is appropriately parameterized.

Computational analyses have been carried out on various derivatives of metallated MT using techniques that range from *ab initio* to molecular mechanics–molecular dynamics (MM-MD) (20–24); however, our group was the first to model the complete apo-βα-rhMT-1a protein with comparison to the individual apo-β and apo-α domains (25). In this study, the metal-free protein was described via two methods: (i) by sequential demetallation to represent the structure following metal ion donation to other proteins or chaperones in the cell, and (ii) by generation of the peptide

sequence as a linear strand to mimic the possible structure following *de novo* synthesis *in vivo*.

Figure 1 shows a series of structural conformations of the individual β and α domains in both ribbon and space-filling representations where the ribbon signifies the protein backbone and the cysteinyl sulfur atoms are shown as yellow spheres.

Figure 1A shows the structures of the individual β and α domains following a one-step removal of all the metal ions without energy minimization to emphasize the configuration of the polypeptide backbone and positioning of the cysteinyl sulfur atoms as they existed in the metallated state but now with all cysteinyl sulfurs protonated. Clearly, the sulfur atoms are all located in the central core of each domain. One-step removal of all of the metal ions is, of course, not chemically reasonable. However, this image provides a view of the metal-free binding site essentially frozen in place by the prior metallation state.

Much more reasonable, and mirroring what can be carried out experimentally, is when the metal-free protein is formed via protonation of the cysteinyl sulfurs with the sequential displacement of each metal ion. In this experiment, the order of proton-induced demetallation was determined on the basis of relative strain energies of each of the metal binding sites, which we have proposed is related to the relative binding constant of each metal. In this way, the most strongly bound metal is displaced last. We then investigated the structural changes of the polypeptide chain and the positioning of the cysteinyl sulfurs with respect to the backbone upon sequential demetallation and compared it with that of the metallated state.

Figure 1B shows the energy-minimized structures of the apo forms of the individual domains of MT produced by the sequential demetallation. Upon removal of the first metal ion, the structure of the remaining partially metallated domain was energy minimized (MM3) prior to a 250-psec MM3/MD calculation at 300 K. The 250-psec conformation was extracted from the dynamics trajectory and energy minimized (MM3). This 250-psec energy-minimized conformation was then used as the starting point for the next sequential demetallation step. This MM3/MD cycle was repeated until all of the metal ions had been removed from the domain, resulting in the metal-free form.

The structural dynamics of the polypeptide backbone of apo-MT was then investigated by carrying out a 5000-psec molecular dynamics calculation (MM3/MD) at 300 K. Thus, Figure 1B shows the energy-minimized β and α domains following sequential removal of the metal ions (0 psec MD) as well as the energy-minimized structures after a 5000-psec MM3/MD calculation at 300 K. Comparison between the domain conformations of apo-MT formed via sequential demetallation (0 psec) and the original conformation established in the metallated state (shown as the one-step removal of the metal ions without MM3 minimization) (Fig. 1A) shows significant alteration to the protein backbone as well as an initial change in position of the cysteinyl sulfurs away from the domain core. This notable change in structure indicates that the binding site cysteines (and therefore the whole peptide chain) of the metallated protein are held in a strained conformation. Under these conditions release of the metal makes the binding site spring open, which we believe rapidly allows for further demetallation because of the increased access to the remaining metals. Experimentally, this is what is seen. When chelators are added to metal-containing MTs, the binding site clusters are disrupted at stoichiometries that are much lower than predicted. This could be energetically desired for facile metal ion donation to metal-free enzymes in the cell.

Even following a 5000-psec MD calculation the protein backbone retains a considerable fraction of the secondary structural features of the metallated species. Significantly, the cysteinyl sulfurs migrate completely to the outside of the peptide. This inversion in Cys-S location exposes these reactive ligands to the environment and presumably allows for facile metallation reactions. Until these calculations had been reported, there had been no information on the possible location of the cysteinyl sulfurs in the apo protein. It is possible that this arrangement, which has a more spherical structure than envisaged from the interpretation of the CD data, allows for the rapid metallation reactions that were measured using stopped-flow kinetic techniques.

The calculations show also that the number of hydrogen bonds in both domains increases upon sequential demetallation, suggesting possible structural stabilization of the resulting demetallated structure via an H-bonding network (26). While the polypeptide backbone structure appeared stable, it was accompanied by a significant degree of flexibility. These unique properties would be advantageous for accommodation of the metal ions as they became coordinated to the inverted cysteinyl sulfurs to form the metal-thiolate cluster within the core of each domain.

We have proposed (26) that the structural conformations and protein backbone dynamics calculated using this technique support the putative functions of MT in metal ion donation as well as in toxic metal sequestration because the protein backbone readily adapts to the degree of metallation, as found for metals such as Cu(I).

Metallation could occur with a peptide that already

→

Figure 1. Ribbon and space-filling representations of (A) metal-free β-rhMT and α-rhMT (Apo formed via one-step demetallation and no MM3 minimization) showing peptide conformation as in the metallated state; (B) energy-minimized (MM3) metal-free β-rhMT and α-rhMT conformations (Apo formed via sequential demetallation) at the 0-psec and 5000-psec time points of a 5000-psec MM3/MD calculation; and (C) energy-minimized (MM3) metal-free β-rhMT and α-rhMT conformations (Apo formed via linear synthesis) at the 5000-psec time point of a 5000-psec MM3/MD calculation. Atom legend: grey = C, blue = N, red = O, yellow = S, green = Cd. Reproduced with permission from Biochem Biophys Res Commun 325: 1271–1278, 2004. Copyright Elsevier (2004) (25). Color figure is available in the on-line version.

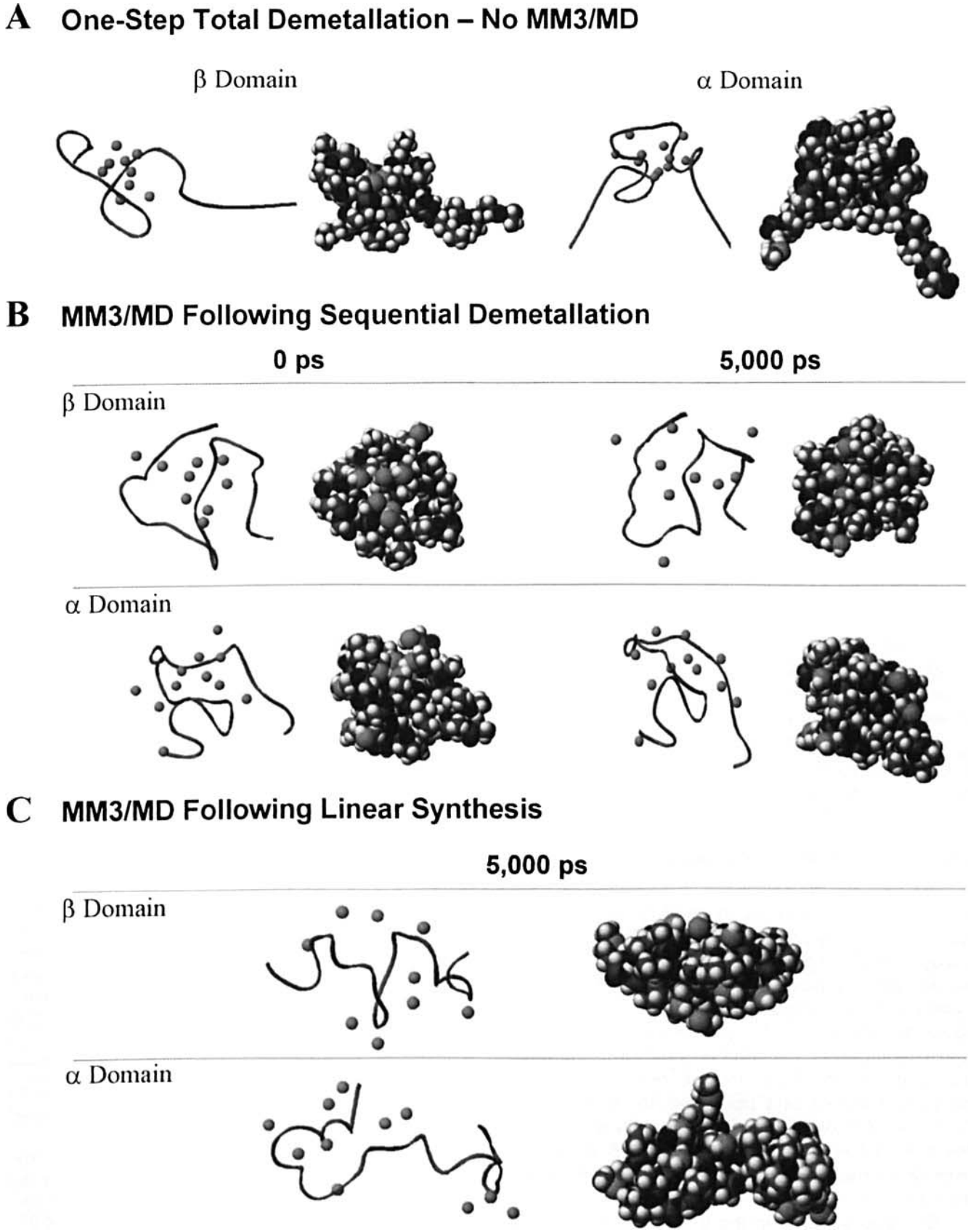
A One-Step Total Demetallation – No MM3/MD
β Domain
α Domain
B MM3/MD Following Sequential Demetallation
0 ps
5,000 ps
β Domain
α Domain
C MM3/MD Following Linear Synthesis
5,000 ps
β Domain
α Domain

exists in the preformed structure described above, or immediately following the synthesis of the peptide, whose structure might be considered to be much less ordered.

Figure 1C shows the energy-minimized apo-β and apo-α domains calculated starting from a synthesized polypeptide strand following a 5000-psec MM3/MD calculation at 300 K. This form of apo-MT differs from the demetallated form of apo-MT in that it is completely linear; or in other words, there is no influence from the previously bound metal ions. Starting from the initial linear conformation mimics the possible conditions following *de novo* synthesis. After the 5000-psec MD, the polypeptide backbone conformation differs significantly from the energy-minimized, sequentially demetallated structure shown in Figure 1A. Structural analysis of the peptide conformations throughout the 5000-psec dynamics calculation showed that no stable conformations of either domain existed; thus properly being called a random coil. Despite this, however, a consistent result is the presence of the cysteinyl sulfurs on the exterior of the domain surface.

It is possible that 5,000 psec is an insufficient length of time to observe any significant folding events; however, preliminary computational studies show that no stable conformations persist during a 15,000-psec MM3/MD calculation, which suggests that *de novo* synthesized apo-MT could still be described as a random coil. The *in vacuo* modeling conditions may also influence the observed protein conformation; however, preliminary studies using a dielectric constant of 78.4 to mimic water still show complete randomness over the 5000-psec dynamics calculation, which is consistent with the previously reported results.

The possibility of the metal-free form of MT contributing to the functions once associated with the metallated protein is an interesting concept and still requires further investigation by both experimental and theoretical methods.

The Mechanism of Metal Binding

We have studied the kinetics of metallation for many years, primarily from the viewpoint of the replacement of metals; for example, the replacement of Zn(II) by Cu(I), Cd(II), and Hg(II). Focusing on the copper reactions, we can ask the following question: If MT initially binds to zinc or cadmium, then can mixed metal species form when Cu(I) is added? Our data answer this question clearly: Cu(I) forms mixed metal clusters with both Cd(II) and Zn(II). However, the details of the Cu(I) binding reactions are very complicated and we have reported on the reactions with the Zn- and Cd-containing protein as well as with the apo fragments. Recently, we have also studied the kinetic properties of reactions of As^{3+} with the isolated, metal-free fragments.

Cu^+ Coordination to the Individual Domains of Metallothionein. The transport, storage, and incorporation of copper into copper-dependent enzymes are vitally important cellular tasks. MT plays a role by binding Cu(I) and making it available to apoenzymes (27, 28). A stoichiometry of six Cu(I) to each of the α and β domains in the Cu-saturated Cu_{12}βα-MT has been reported from spectroscopic and analytical measurements (29–31). However, the mechanism by which the Cu(I) forms the clusters and then is sequestered by apoenzymes is not understood and few kinetic data are currently available.

Cu(I) coordinated to the cysteine thiolate ligands of MT generates a highly specific emission profile observed near 600 nm upon excitation at 280 nm. This property provides an ideal probe with which to interrogate the structure of the $Cu\text{-}S_{cys}$ binding site in MT. This sensitivity, then, is a marker for rearrangement occurring in the Cu binding site: increased solvent access will reduce the intensity, whereas a tighter cage structure will exclude the surrounding solvent, resulting in increased intensity. In addition, the wavelength of the emission is dependent on the exact environment around the Cu(I). For example, the coordination number (two, three, or four), and the nearest neighbor (a terminal or bridging Cys sulfur) will influence the emission wavelength, making this an invaluable tool for probing the Cu(I)-thiolate cluster arrangement.

Overall, the emission intensity observed for the Cu_nβ cluster (n = 1–6) is approximately 45% less than the emission intensity of the comparable Cu_nα (n = 1–6) cluster. This difference in relative quantum yield between the copper-substituted α and β domains leads us to conclude that the Cu_6β cluster must have a more porous structure than the Cu_6α cluster, which allows for greater solvent accessibility, and therefore, lower quantum yields, a property that has been predicted in the proposed Cu_6S_9-β structure.

The emission intensity differences that exist between the two domains, and between each Cu_n cluster, provide a structure-dependent property that can be correlated to the copper composition of a Cu_nα or Cu_nβ cluster being formed. The λ_{max} shifts from 594.5 up to 600.5 nm for Cu^+ bound to the β domain of MT, up to the filled Cu_6β-MT cluster, and from 603.5 up to 606.5 nm for Cu^+ bound to the α domain

Table 1. Relative intensity (%) of each Cu_n-α and Cu_n-β MT cluster relative to a Cu_6-α MT species and their corresponding wavelengths. Reproduced with permission from Biochem Biophys Res Commun 318: 73–80, 2004. Copyright Elsevier (2004) (32).

Mol Cu(I) added	Relative Intensity (%)		Wavelength (nm)	
n	Cu_n-α MT	Cu_n-β MT	Cu_n-α MT	Cu_n-β MT
0	0	0	—	—
1	12.45	4.25	603.50	594.50
2	27.04	8.03	604.00	594.98
3	37.98	13.85	604.33	595.98
4	55.21	24.31	605.33	598.97
5	78.84	39.46	606.32	599.81
6	100.00	44.20	606.50	600.48

of MT, up to the filled $Cu_6\alpha$-MT cluster. Consequently, the λ_{max} differences that exist between the two domains provide a sensitive structure-dependent property that can be correlated with the location of copper ions as either in the α or the β domain of MT. Together, the emission intensity and λ_{max} become parameters with which to monitor the distribution of Cu^+ ions between the α and β domains of MT as a function of time when both domains are present.

Addition of Cu(I) to $Cd_3\beta$-rhMT-1a and $Cd_4\alpha$-rhMT-1a fragments results in Cu,Cd mixtures that exhibit unique emission spectral parameters, defined by specific emission intensities and band maxima (λ_{max} values); these data are summarized in Table 1. Using extensive simulations that combined the specific emission intensity and λ_{max} values for a wide range of Cd,Cu_n-α and Cd,Cu_n-β cluster combinations, we were able to identify the particular emission intensity and band maximum of a single species observed over time during the mixing of $Cu_6\beta$-rhMT-1a with $Cd_4\alpha$-rhMT-1a and $Cu_6\alpha$-rhMT-1a with $Cd_3\beta$-rhMT-1a. These simulations allowed for identification of the Cu and Cd compositions that exist in the α and β domains of MT at specific time intervals during these mixing experiments.

The spectroscopic data show that Cu^+ changes its binding site after first binding to the Cys residues of MT. When copper-containing fragments are mixed with the cadmium-containing partner fragment (e.g., Cu_6-α MT with Cd_3-β MT or Cu_6-β MT with Cd_4-α MT) the copper will redistribute. By combining the λ_{max} and emission intensities with the reaction time we can construct figures that track the changes in both band maximum and band intensity with time. The identification of the particular species comes from analysis of the spectral data of the single fragments when complexed with Cd(II) and Cu(I) (32). Figure 2A and B summarize the change in Cd,Cu composition in the α and β domains of MT as a function of time following the mixing of $Cu_6\beta$-MT with $Cd_4\alpha$-MT and $Cu_6\alpha$-MT with $Cd_3\beta$-MT.

We can test the relative binding constants of the β and α domains using mixing experiments. When $Cu_6\alpha$-MT is mixed with $Cd_3\beta$-MT there is a rapid decline in emission intensity that is also connected with a blue shift in λ_{max} so that at 1000 secs the final product of the mixing reaction is identified as a mixture of $Cu_4Cd_{3-n}\beta$-MT and $Cu_2Cd_n\alpha$-MT, which has an intensity of 33% when compared with the initial emissive species and a λ_{max} of 597.5 nm. The rapid and continuing decrease in emission intensity with time clearly can be correlated with migration of Cu^+ ions from the α domain to the less emissive β domain. The reaction required more than one step when fitted: the parameters include a rapid Cu^+ transfer rate of $\sim 2 \times 10^{-1}$ s^{-1} and a slower rate of $\sim 8 \times 10^{-3}$ s^{-1}. The faster rate indicates an immediate transfer of Cu^+ ions from the α to the β domain, a kinetically driven process, while the second rate can be correlated with the redistribution of Cu^+ ions within the new cluster, a thermodynamically driven process.

The converse experiment, mixing $Cu_6\beta$-MT with $Cd_4\alpha$-MT, tests the relative binding constants for Cu^+ redistributing from the β domain into the occupied α domain. In this experiment there is a slower blue shift in λ_{max} so that at 1000 secs the final product of the mixing reaction is identified as a mixture of $Cu_{4-5}Cd_n\beta$-MT and $Cu_{1-2}Cd_{4-n}\alpha$-MT, with an intensity of 69% when compared with the starting emissive species and a wavelength of 598 nm. We have proposed that the slower decline in emission intensity is due to the less rapid migration of Cu^+ from the less emissive β domain to the more emissive α domain. The kinetic data were fitted to a single exponential decay function describing a single-step reaction process with a rate of $\sim 8 \times 10^{-3}$ s^{-1}.

It has been shown previously that following mixing of Zn_7-MT and Cd_7-MT there is a slow metal redistribution

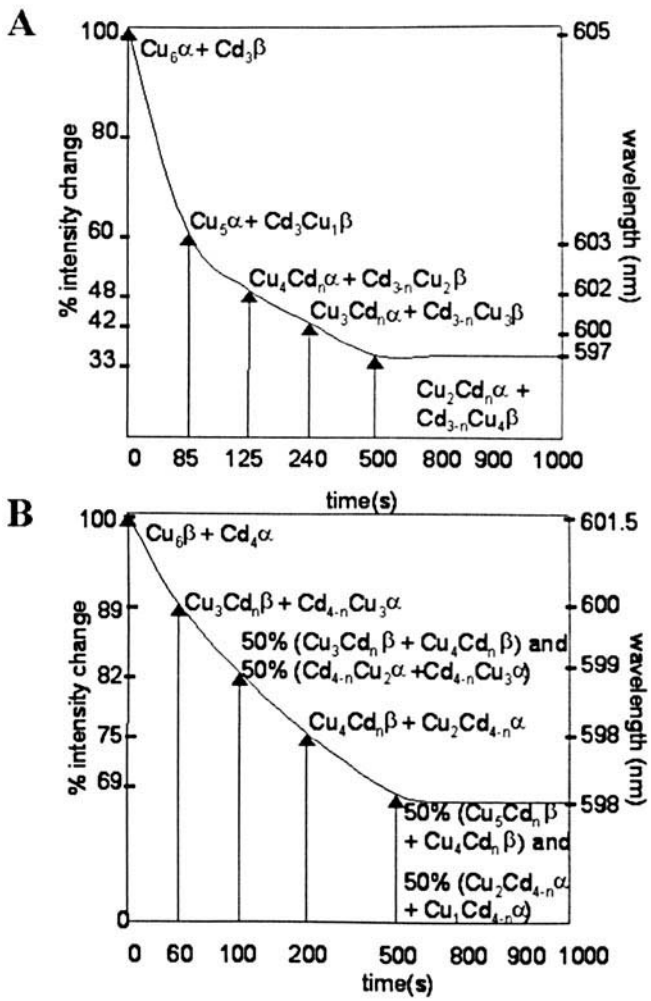

Figure 2. Calculated Cu and Cd distributions in the mixed α- and β-MT species found at several time intervals during the mixing experiment of (A) $Cu_6\beta$-MT with $Cd_4\alpha$-MT and (B) $Cu_6\alpha$-MT with $Cd_3\beta$-MT. The compositions were determined by calculating the λ_{max} and emission intensity for all possible compositions of Cu_n-α and Cu_n-β cluster species that would yield a minimal difference between the experimental data carried out by using data summarized in Table 1. Species found in solution are 100% unless otherwise stated. (The time on the x-axis is not to scale). Reproduced with permission from Biochem Biophys Res Commun 318: 73–80, 2004. Copyright Elsevier (2004) (32).

process between the domains as formation of thermodynamically stable, mixed-metal products occurs. Therefore, in this scenario we correlate the distribution of Cu^+ from the β to the α domain to be a similar process, in which the thermodynamically stable, mixed-metal Cd,Cu-β and Cd,Cu-α products form. These data clearly show that Cu^+ redistributes between the domains so that neither reaction forms the fully metallated Cu_6 cluster at t_∞ because the wavelengths of the final products do not match the wavelength of the associated Cu_6 cluster (600.5 nm for a $Cu_6\beta$ cluster and 603.5 nm for a $Cu_6\alpha$ cluster).

According to the simulated spectral data (emission intensities and λ_{max}) shown in Figure 2, only a few cluster compositions are possible. The $Cu_4\beta$ cluster is prominent in both mixing experiments. This strongly suggests that the $Cu_4\beta$ cluster could be a possible intermediate required for the formation of the $Cu_6\beta$ cluster in the presence of low copper concentrations. That Cu^+ preferentially binds to the β domain (from the higher Cu^+ stoichiometry found in that domain by the end of each mixing experiment) provides the first spectroscopic evidence of the β domain preference that complements the experiments carried out using biochemical techniques by Winge in the mid 1980s (30, 31). Although the presence of a Cu_4 cluster intermediate in the β domain has been identified from previous copper binding studies of Zn_7-MT, it has not been previously linked to the Cu^+ exchange phenomena between the α and β domains.

This observation supports the idea that a $(Cu_6\alpha)(Cu_6\beta)$-MT species would be unlikely *in vivo* under conditions of low Cu^+ concentrations because native Zn_7-MT synthesized by mammals exposed to metals such as Cu^+ always yielded mixed-metal clusters that contained Zn^{2+} ions (33–35). Mass spectrometry studies of Cu^+ binding to Zn_7- and Cd_7-MT have shown the presence of mixed-metal species (30, 31), but no stoichiometric distribution of Cu^+ between the α and β domains of MT could be observed as a function of time, as has been possible in this study.

As^{3+} Coordination to the Individual Domains of MT. Previous studies carried out on the arsenic metallation of mammalian MT have shown that six As(III) atoms coordinate to the two-domain protein (36, 37), however, the distribution of the As(III) between the α and β domains and the ligand environment around each As(III) has yet to be proven. Examination of well-characterized As^{3+}-thiolate complexes such as $[Cp^*_2Ru_2As_4S_4]$ (38) and $[Pt(As_3S_5)_2]^{2-}$ (39) show a predominantly distorted trigonal pyramidal geometry, thus we propose that three As^{3+} ions bind to each of the individual domain fragments of mammalian MT on the basis of a one As^{3+} to three S_{cys} ratio.

Using electrospray ionization–mass spectrometry (ESI-MS), we show that each individual domain fragment of the recombinant human MT-1a binds three As^{3+} ions in a ratio of one As^{3+} to three S_{cys} (40). This stoichiometry is easily explained for the β domain because all nine of the cysteinyl sulfurs are involved in the coordination of the three As^{3+} ions. However, in the case of the α domain, we still only observe a maximum of three coordinated As^{3+} ions, even in the presence of excess As^{3+}. In keeping with the one As^{3+} to three S_{cys} ratio, we propose that the three As^{3+} ions coordinate to nine of the 11 cysteines in the α domain, leaving the remaining two cysteine residues protonated. We interpret these results to mean that cluster formation (that is, metal-thiolate bonding involving bridging thiolates) is not occurring.

Use of temperature- and time-resolved ESI-MS allowed for the complete kinetic analysis of the individual MT domain fragments (40). Figure 3 shows a three-dimensional (3-D) plot constructed from the temperature-resolved ESI-MS experimental data, which was used to obtain rate constants, activation energies, activation enthalpies, and activation entropies. These 3-D plots illustrate the trend of As^{3+} metallation as a function of time and temperature. From Figure 3, we observe that As_3-H_2-αMT at low temperatures and short reaction times is near 0% abundance; however, as time progresses and the temperature rises, the abundance of As_3-H_2-αMT steadily increases until it reaches a maximum of 100% abundance at the longest reaction time of 1020 secs and the highest temperature of 84°C. As_3-H_2-αMT and As_3-βMT have been shown in the previous study to be the final product for the reaction of As^{3+} with the individual domains of MT. The metallation pathway of each domain can be described by three sequential noncooperative bimolecular reactions in which each of the three As^{3+} ions are coordinated to three cysteine thiolate ligands. This mechanistic scheme for α MT is illustrated in Figure 4, where the results of the analysis use a model with three sequential bimolecular reactions. As_1H_8-αMT and As_2H_5-αMT are considered intermediate species in this mechanism and are consumed in the formation of the final product, As_3H_2-αMT.

Table 2 lists the rate constants and activation energies for the each of the three sequential metallation steps of both the α and β domains at 25°C. Analysis of these kinetic results shows that As^{3+} metallation occurs more rapidly within the α domain than the β domain. Binding of the first As^{3+} ion occurs readily; however, the binding of the second and, especially the third As^{3+}, are slower. A possible explanation for this is the way the peptide wraps around the As^{3+} ions and the lack of cluster formation. As mentioned earlier, we postulate that As^{3+} binding occurs with sequestration of the As^{3+} ions by terminally coordinated cysteines rather than via formation of a metal-thiolate cluster consisting of both bridging and terminal cysteine residues. Evidence for this can be seen in the lack of an As_4-αMT species where bridging cysteines would accommodate this metal-binding stoichiometry.

Kinetic characterization of As^{3+} metallation to MT has provided insight into the structure of MT relative to metals such as Cd(II), Zn(II), and Cu(I).

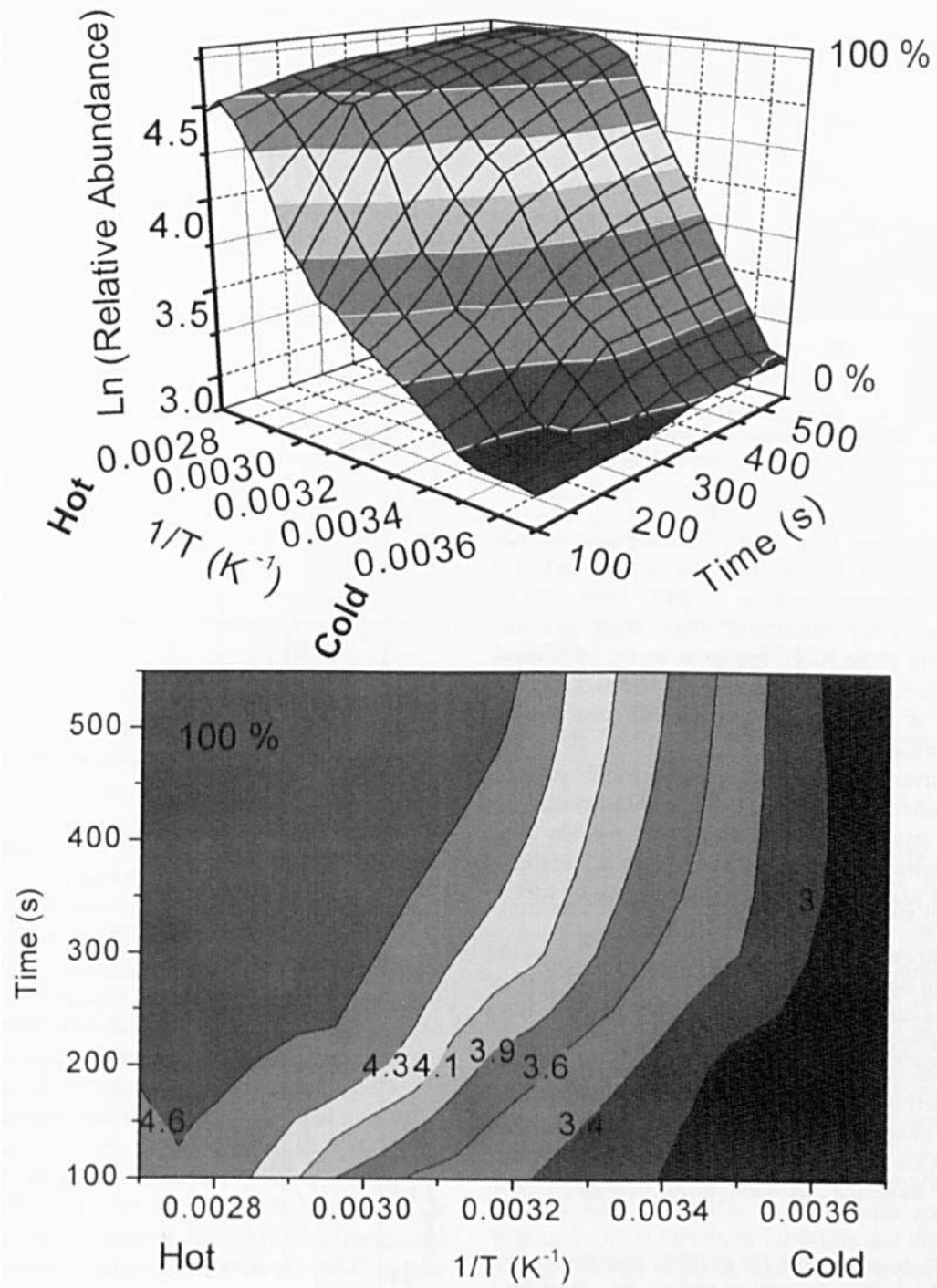

Figure 3. Three-dimensional plot showing formation of As_3H_2-α-rhMT as a function of time and temperature by ESI-MS. This is the final species in the reaction between As^{3+} and apo-αMT. Reproduced with permission from J Am Chem Soc 128 (in press), 2006. Copyright American Chemical Society (2006) (40).

Using XAFS Spectra as an Aid to Predict Metal Binding Sites via Computational Methods

Metalloproteins play structural, storage, and catalytic roles. Determination of the coordination geometries of the metal centers is particularly important for the elucidation of reaction mechanisms, as the proximity of the atoms and the accessibility to the atoms often determines the outcome and overall selectivity of the reaction. However, structural information for a metal bound to amino acid ligands that are part of a long polypeptide chain is difficult to obtain.

We have shown that XAS spectroscopy can be used in conjunction with molecular modeling to effectively determine the identities of the coordinating ligand atoms and their geometric parameters, and hence predict the coordination geometries at the metal binding sites (41). While the extended x-ray absorption fine structure (EXAFS) portion of

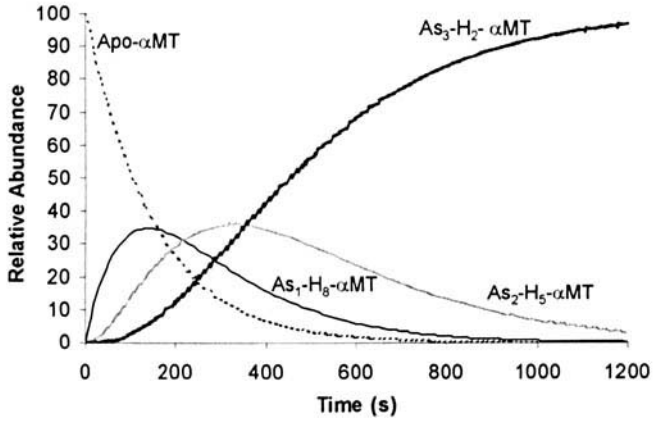

Figure 4. Model showing the sequential As^{3+} metallation of the α domain of MT at 303 K. Reproduced with permission from J Am Chem Soc 128 (in press), 2006. Copyright American Chemical Society (2006) (40).

the XAFS spectrum has been widely used, the most accurate parameter derived is that of the bond length, and in a multimetal environment such as in MT, these will be averaged. The x-ray absorption near edge structure (XANES) region of the XAFS spectrum, on the other hand, is very sensitive to the 3-D environment as far as 5 Å away. The problem is in analyzing the XANES data due to multiple scattering effects.

Recent advances in the use of the FEFF program (version 8.2 software package [42, 43]) and the availability of molecular modeling programs that can provide good estimates of metal-amino acid bonding, have introduced a new means of examining the metal binding site or sites in metalloproteins.

The key to our work with MT is that XANES data can be collected for both protein and model compounds, and the FEFF program can successfully simulate the major features in the XAFS spectrum from atomic coordinates of the absorbing metal and its surrounding ligands using *ab initio* multiple scattering calculations. The required coordinates can now be obtained from molecular models calculated using the CAChe Worksystem Pro 6.1.1 (Fujitsu America), or any other modeling software, using best-guess coor-

Table 2. Rate constants (k) at 25°C and activation energies (E_A) for the formation of As_1, As_2, and As_3 species for each of the α and β domains of MT. Reproduced with permission from J Am Chem Soc 128 (in press), 2006. Copyright American Chemical Society (2006) (40).

Arsenic species	k at 25°C ($M^{-1}s^{-1}$)	E_A (kJ mol^{-1})
As_1-H_6-βMT	3.6	32
As_2-H_3-βMT	2.0	35
As_3-βMT	0.8	29
As_1-H_8-αMT	5.5	33
As_2-H_5-αMT	6.3	29
As_3-H_2-αMT	3.9	23

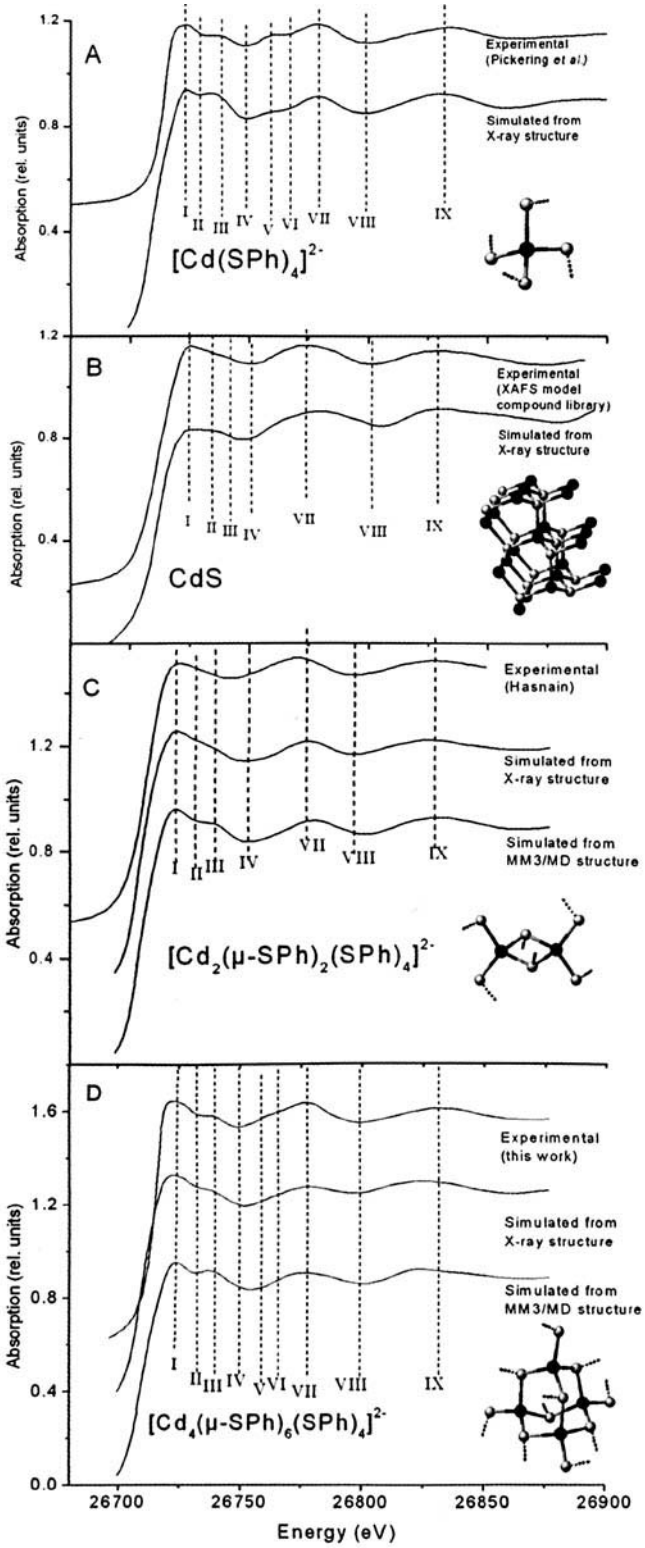

Figure 5. Comparison of simulated XAFS spectra corresponding to cadmium-thiolate complexes to experimental XAFS spectra. (A) $[Cd(SPh)_4]^{2-}$, (B) CdS, (C) $[Cd_2(\mu\text{-}SPh)_2(SPh)_4]^{2-}$, and (D) $[Cd_4(\mu\text{-}SPh)_6(SPh)_4]^{2-}$. Reproduced with permission from Inorg Chem 44:4923–4933, 2005. Copyright American Chemical Society (2005) (41).

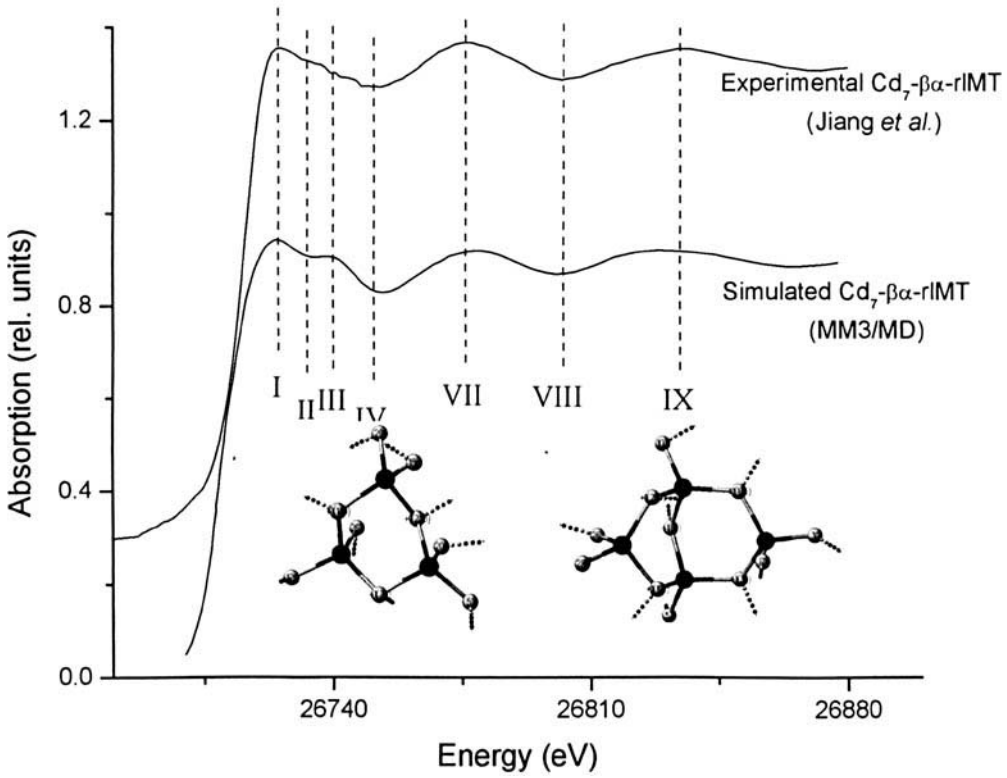

Figure 6. Comparison of experimental and simulated XAFS spectra for Cd_7–βα-rIMT. Reproduced with permission from Inorg Chem 44:4923–4933, 2005. Copyright American Chemical Society (2005) (41).

dinates as starting parameters (i.e., from x-ray diffraction or NMR data).

We have used the coordinates of Cd-thiolate model compounds and Cd_7-βαMT from MM3/MD calculations as input for the FEFF program, which we used to simulate the Cd K-edge XAFS spectra for both the simple cadmium-thiolate complexes (Fig. 5) and for rabbit liver MT (Fig. 6). Each simulated spectrum was compared with experimental spectra to determine the accuracy of the cluster geometries and bonding. In each spectrum we have labeled nine major features that can be associated between all spectra, for simplicity of comparison. The simplest cases are $[Cd(SPh)_4]^{2-}$ (Fig. 5A) and CdS (Fig. 5B), for which we have compared their simulated spectra with experimental data from Pickering *et al.* (44) and from the XAFS model compound library (45), respectively. There is a minor overemphasis of Feature III; however, the correlation in energies and intensities indicates that FEFF can successfully predict experimental XAFS spectra.

Calculated MM3/MD structures for the $[Cd_2(\mu\text{-}SPh)_2(SPh)_4]^{2-}$ and $[Cd_4(\mu\text{-}SPh)_6(SPh)_4]^{2-}$ were compared with corresponding x-ray structures, and were found to have comparable geometric attributes. XAFS simulations using both sets of coordinates were then compared with experimental data proposed by Hasnain (unpublished) (Fig. 5C) and with experimental data that we measured (Fig. 5D), respectively. Again, we observe comparable energies and intensities between simulated spectra and experimental spectra. These data show that MM3/MD calculated structures give similar spectroscopic accuracies to the x-ray structures.

Figure 6 shows an XAFS spectrum simulated from an MM3/MD energy-minimized structure of rabbit liver Cd_7-βα-rIMT-2a (where the spectrum shown is an average of the spectra for the individual β and α domains) and the corresponding experimental XAFS spectrum measured by Jiang *et al.* (46). Here, we observe very good correlation between the energies and intensities of the features.

This work demonstrates that simulations of the spectroscopic properties at the metal sites in model structures allows structural validation and has very promising applications to the field of structural prediction.

Determination of the Metal Binding Stoichiometry for the Novel *Fucus vesiculosus* MT

Although the mammalian MTs are well known, MTs from other sources are poorly characterized. MT has been reported from an extremely wide range of organisms. We have recently studied the MT from the seaweed *Fucus vesiculosus*, which has a sequence with 16 cysteine residues, arranged in groups of seven and nine. This seaweed is unusual when compared with other algal species in that it can survive in toxic metal–contaminated aquatic environments. The MT gene has been identified in *Fucus vesiculosus* by

Kille and coworkers (15), which suggests a possible protective mechanism against toxic metals for this species.

The metal-binding properties of the recombinant *F. vesiculosus* MT (rfMT) were determined using a combination of UV absorption, CD, and electrospray mass spectral techniques. The overall metal-to-sulfur ratios of this novel algal protein when bound to divalent cadmium and zinc were determined to be Cd_6S_{16} and Zn_6S_{16}, respectively. Mixed Cd/Zn species were also formed when Cd^{2+} was added to the Zn-containing Fucus MT. Only one conformation was identified at low pH for the native protein corresponding to the metal-free protein. Analysis of the UV absorption, CD, and ESI-MS data indicate that rfMT binds six Cd^{2+}, Zn^{2+}, or combinations of both metal atoms. On the basis of pH titrations in the UV absorption, CD, and ESI-MS experiments, we conclude that the Cd_3S_7 domain is present and much less stable than the Cd_3S_9 domain. The Cd_3S_7 structure represents a previously unknown metal-to-cysteine ratio in an MT and will involve extensive bridging for the coordinating cysteine sulfurs.

Summary

Studies of the metal-binding properties of MTs have been described for more than 30 years since the earliest reports by Kagi and Vallee (47–49). Many different techniques have been used, each bringing new information concerning the properties of these remarkable proteins. In this review we have described the current status of metal binding using mechanistic and structural techniques. Clearly, there is much to learn about the control imparted on the metal-binding site by the peptide in MT.

Recent x-ray diffraction results for the copper-containing yeast protein (50) provided firm evidence for mixed coordination geometries, supporting conclusions reached many years ago on the basis of analysis of CD and emission data. Yet this x-ray diffraction result is only the second in 30 years, so for progress to be made, methods using techniques such as XANES are required. These methods provide metal-dependent data that cannot be obtained directly from NMR experiments, allowing the structures of a large number of proteins to be proposed.

The mechanistic information about these metallation reactions is at a very early stage of development, but they clearly represent essential information.

1. Kagi JHR, Nordberg M, Eds. Metallothionein I. Basel: Birkhauser Verlag, 1979.
2. Kagi JHR, Kojima Y, Eds. Metallothionein II. Basel: Birkhauser Verlag, 1987.
3. Klaassen CD, Ed. Metallothionein IV. Basel: Birkhauser Verlag, 1997.
4. Suzuki KT, Imura N, Kimura M, Eds. Metallothionein III. Basel: Birkhauser Verlag, 1993.
5. Riordan JF, Vallee BL. Methods in Enzymology. San Diego: Academic Press, Vol 205:p681, 1991.
6. Stillman MJ, Shaw III CF, Suzuki KT. Metallothioneins: synthesis, structure and properties of metallothioneins, phytochelatins and metal-thiolate complexes. New York: VCH Publishers, Inc., 1992.
7. Stillman MJ. Metallothioneins. Coord Chem Rev 144:461–511, 1995.
8. Miles AT, Hawksworth GM, Beattie JH, Rodilla V. Induction, regulation, degradation, and biological significance of mammalian metallothioneins. Crit Rev Biochem Mol Biol 35:35–70, 2000.
9. Yang Y, Maret W, Vallee BL. Differential fluorescence labelling of cysteinyl clusters uncovers high tissue levels of thionein. Proc Natl Acad Sci U S A 98:5556–5559, 2001.
10. Bagla P. Arsenic-laced well water poisoning Bangladesh. National Geographic News. Available at: http://news.nationalgeographic.com/news/2003/06/0605_030605_arsenicwater.html. Accessed August 2006.
11. Hug S, Wegelin M, Gechter D, Canonica L. Arsenic contamination of ground water: disastrous consequences in Bangladesh. EAWAG News 49:18–20, 2000.
12. Demel S, Shi J, Martin P, Rosen BP. Arginine 60 in the ArsC arsenate reductase of *E. coli* plasmid R773 determines the chemical nature of the bound As(III) product. Protein Sci 13:2330–2340, 2004.
13. Leach AR. Molecular modelling: principles and applications. Harlow, England: Prentice Hall, p720, 2001.
14. Schlick T. Molecular modeling and simulation: an interdisciplinary guide. New York: Springer-Verlag, p634, 2002.
15. Morris CA, Nicolaus B, Sampson V, Harwood JL, Kille P. Identification and characterization of a recombinant metallothionein protein from a marine alga, *Fucus vesiculosus*. Biochem J 338:553–560, 1999.
16. Robbins AH, McRee DE, Williamson M, Collett SA, Xuong NH, Furey WF, Wang BC, Stout CD. Refined crystal structure of cadmium-zinc metallothionein at 2.0 Å resolution. J Mol Biol 221:1269–1293, 1991.
17. Arseniev A, Schultze P, Worgotter E, Braun W, Wagner G, Vasak M, Kagi JHR, Wuthrich K. Three-dimensional structure of rabbit liver [Cd_7]metallothionein-2a in aqueous solution determined by nuclear magnetic resonance. J Mol Biol 201:637–657, 1988.
18. Otvos JD, Armitage IM. Structure of the metal clusters in rabbit liver metallothionein. Proc Natl Acad Sci U S A 77:7094–7098, 1980.
19. Shapiro SG, Squibb KS, Markowitz LA, Cousins RJ. Cell-free synthesis of metallothionein directed by rat liver polyadenylated messenger ribonucleic acid. Biochem J 175:833–840, 1978.
20. Enescu M, Renault J-P, Pommeret S, Mialocq J-C, Pin S. Ab initio study of Cd-thiol complexes: application to the modelling of the metallothionein active site. Phys Chem Chem Phys 5:3762–3767, 2003.
21. Chang C-C, Huang PC. Semi-empirical simulation of Zn/Cd binding site preference in the metal binding domains of mammalian metallothionein. Protein Eng 9:1165–1172, 1996.
22. Berweger CD, Theil W, van Gunsteren WF. Molecular-dynamics simulation of the beta domain of metallothionein with a semi-empirical treatment of the metal core. Proteins 41:299–315, 2000.
23. Fowle DA, Stillman MJ. Comparison of the structures of the metal-thiolate binding site in Zn(II)-, Cd(II)-, and Hg(II)-metallothioneins using molecular modeling techniques. J Biomol Struct Dyn 14:393–406, 1997.
24. Presta A, Fowle DA, Stillman MJ. Structural model of rabbit liver copper metallothionein. J Chem Soc Dalton Trans 6:977–984, 1997.
25. Rigby KE, Stillman MJ. Structural studies of metal-free metallothionein. Biochem Biophys Res Comm 325:1271–1278, 2004.
26. Rigby KE, Stillman MJ. Molecular dynamics study on the folding and metallation of the individual domains of metallothionein. Proteins 62: 159–172, 2006.
27. Petering DH, Fowler BA. Roles of metallothionein and related proteins in metal metabolism and toxicity: problems and perspectives. Environ Health Perspect 65:217–224, 1986.
28. Aggett PJ, Barclay SM. Neonatal trace element metabolism. In: Cowett

RM, Ed. Principles of Perinatal-Neonatal Metabolism. New York: Springer-Verlag, pp500–530, 1991.

29. Green AR, Presta A, Gasyna Z, Stillman MJ. Luminescence probe of copper-thiolate cluster formation within mammalian metallothionein. Inorg Chem 33:4159–4168, 1994.
30. Nielson KB, Winge DR. Order of metal binding in metallothionein. J Biol Chem 258:13063–13069, 1983.
31. Nielson KB, Winge DR. Preferential binding of copper to the beta domain of metallothionein. J Biol Chem 259:4941–4946, 1984.
32. Salgado MT, Stillman MJ. Cu(I) distribution in metallothionein fragments. Biochem Biophys Res Comm 318:73–80, 2004.
33. Briggs RW, Armitage IM. Evidence for site-selective metal binding in calf liver metallothionein. J Biol Chem 257:1259–1262, 1982.
34. Bremner I, Young BW. Isolation of (copper, zinc)-thioneins from the livers of copper-injected rats. Biochem J 157:517–520, 1976.
35. Bremner I, Young BW. Isolation of (copper, zinc-) thioneins from pig liver. Biochem J 155:631–635, 1976.
36. Jiang G, Gong Z, Li X-F, Cullen WR, Le XC. Interaction of trivalent arsenicals with metallothionein. Chem Res Toxicol 16:873–880, 2003.
37. Toyama M, Yamashita M, Hirayama N, Murooka Y. Interactions of arsenic with human metallothionein-2. J Biochem (Tokyo) 132:217–221, 2002.
38. Brunner H, Nuber B, Poll L, Roidl G, Wachter J. Novel inorganic cage structures based on AsS ligands and cyclopentadienylruthenium groups. Chem-Eur J 3:57–61, 1997.
39. Chou J-H, Kanatzidis MG. Pt(II) vs Pt(IV) in AsS_3^{3-} solutions and isolation of the clusters $[Pt(As_3S_5)_2]^{2-}$ and $[Pt_3(AsS_4)_3]^{3-}$. Observation of unique thioarsenate ligands and Pt-As bonds. Inorg Chem 33:5372–5373, 1994.
40. Ngu TT, Stillman MJ. The kinetics of arsenic binding to metallothionein. J Am Chem Soc 128 (39) (in press), 2006.
41. Chan J, Merrifield ME, Soldatov AV, Stillman MJ. XAFS spectral analysis of the cadmium coordination geometry in cadmium thiolate clusters in metallothionein. Inorg Chem 44:4923–4933, 2005.
42. Ankudinov AL, Ravel B, Rehr JJ, Conradson SD. Real-space multiple-scattering calculation and interpretation of x-ray-absorption near-edge structure. Phys Rev B 58:7565–7576, 1998.
43. Ankudinov AL, Bouldin CE, Rehr JJ, Sims J, Hung H. Parallel calculation of electron multiple scattering using Lanczos algorithms. Phys Rev B 65:104–107, 2002.
44. Pickering IJ, Prince RC, George GN, Rauser WE, Wickramasinghe WA, Watson AA, Dameron CT, Dance IG, Fairlie DP, Salt DE. X-ray absorption spectroscopy of cadmium phytochelatin and model systems. Biochim Biophys Acta 1429:351–364, 1999.
45. Newville M, Carroll S, O'Day P, Waychunas G. The XAFS Model Compound Library. Available at: http://cars9.uchicago.edu/~newville/ModelLib/. Accessed August 2004.
46. Jiang DT, Heald SM, Sham TK, Stillman MJ. Structures of the cadmium, mercury, and zinc thiolate clusters in metallothionein—XAFS study of Zn_7-MT, Cd_7-MT, Hg_7-MT, and Hg_{18}-MT formed from rabbit liver metallothionein-2. J Am Chem Soc 116:11004–11013, 1994.
47. Kagi JHR, Vallee BL. Metallothionein: a cadmium and zinc-containing protein from equine renal cortex. II. Physicochemical properties. J Biol Chem 236:2435–2442, 1961.
48. Kagi JHR, Vallee BL. Metallothionein: a cadmium- and zinc-containing protein from equine renal cortex. J Biol Chem 235:3460–3465, 1960.
49. Kojima Y, Berger C, Vallee BL, Kagi JHR. Amino-acid sequence of equine renal metallothionein-1B. Proc Natl Acad Sci U S A 73:3413–3417, 1976.
50. Calderone V, Dolderer B, Hartmann HJ, Echner H, Luchinat C, Bianco CD, Mangani S, Weser U. The crystal structure of yeast copper thionein: the solution of a long-lasting enigma. Proc Natl Acad Sci U S A 102:51–56, 2005.